



**Calhoun: The NPS Institutional Archive**  
**DSpace Repository**

---

Theses and Dissertations

1. Thesis and Dissertation Collection, all items

---

1967-12

# Investigation of shear lag in heat exchanger module

Machado, Robert Francis

Monterey, California. U.S. Naval Postgraduate School

---

<http://hdl.handle.net/10945/12488>

---

This publication is a work of the U.S. Government as defined in Title 17, United States Code, Section 101. Copyright protection is not available for this work in the United States.

*Downloaded from NPS Archive: Calhoun*



<http://www.nps.edu/library>

Calhoun is the Naval Postgraduate School's public access digital repository for research materials and institutional publications created by the NPS community. Calhoun is named for Professor of Mathematics Guy K. Calhoun, NPS's first appointed -- and published -- scholarly author.

**Dudley Knox Library / Naval Postgraduate School**  
**411 Dyer Road / 1 University Circle**  
**Monterey, California USA 93943**

NPS ARCHIVE  
1967  
MACHADO, R.

INVESTIGATION OF SHEAR LAG IN HEAT  
EXCHANGER MODULE

ROBERT FRANCIS MACHADO








INVESTIGATION OF SHEAR LAG IN HEAT EXCHANGER MODULE

by

Robert Francis Machado  
Captain United States Marine Corps  
B.S., California State Polytechnic College, 1960



Submitted in partial fulfillment of the  
requirements for the degree of

MASTER OF SCIENCE IN AERONAUTICAL ENGINEERING

from the

NAVAL POSTGRADUATE SCHOOL  
December 1967

# ABSTRACT

Results of a photoelastic model test which simulates the junction of the closure bar with sheet of a heat exchanger are presented. Values of shear stress 30 per cent above predicted values were found to exist. A linear technique for determination of maximum shearing stress is presented for the purpose of design. Qualitative techniques were employed to compare the results of tests of various photoelastic models.

TABLE OF CONTENTS

	Page
List of Tables	5
List of Illustrations	7
List of Symbols	9
Acknowledgement	11
Introduction	13
The Model	17
Equipment and Procedure	20
Discussion	25
Conclusions and Recommendations	30
Bibliography	32
Appendix A: Fabrication of the Models	34
Appendix B: Calibration of Model Material	36
Appendix C: Determination of the Portion of the Load Transmitted as Tension	38





## LIST OF TABLES

<u>Table</u>		<u>Page</u>
I	Summary-Model/Prototype Relationship	40
II	Four Arrangements of the Optical Elements in a Circular Polariscopes	41
III	Photoelastic Color Stress Conversion Table	42
IV	Model Materials	44
V	Mechanical Properties of Photoelastic Materials	44
VI	List of Equipment	45
VII	Calibration of Material	45



## LIST OF ILLUSTRATIONS

### Figure

1. Idealized Shear Lag Model
2. Plastic Shear Lag Model Type 1
3. Plastic Shear Lag Model Type 2
4. Plastic Shear Lag Model Type 3
5. Experimental Setup
6. Principal Axis Orientation, Contours of Constant
7. Model Load Adapter
8. Integral Order Fringe Pattern Model Type 2
9. Half Order Fringe Pattern Model Type 2
10. Shear Distribution in Sheet Along Left Closure Bar
11. Shear Distribution in Sheet Along Right Closure Bar
12. Comparison of Predicted Shear Stress Levels with  
Experimental Results
13. Composite Fringe Patterns
14. Integral Order Fringe Pattern Model Type 1,  
250 Pounds
15. Half Order Fringe Pattern Model Type 1, 250 Pounds
16. Integral Order Fringe Pattern Model Type 3,  
280 Pounds
17. Half Order Fringe Pattern Model Type 3, 280 Pounds
18. General Dimensions
  - A Actual Bar and Sheet Detail
  - B Analysis Model



## LIST OF SYMBOLS

The following is a list of symbols and abbreviations used in this paper. Exceptions are defined in the text where appropriate.

e	Naperian logarithmic base
h	Height (inches)
psi	Pounds per square inch
w	Width (inches)
x	Lateral direction, in the plane of the sheet
y	Longitudinal direction, in the plane of the model
C	Stress optic coefficient (psi/fringe/inch)
K	A suitable constant, appropriately defined in text
P <sub>0</sub>	A general applied loading (pounds)
€	Incremental unit
θ	Angle between the principal axis system and the geometric axis system of the model (degrees)
σ	Normal stress component (psi)
τ	Shear stress component (psi)

### Subscripts

ave	average
i	Discrete point, the ith point
max	Maximum
x	Related to the direction of the x axis
y	Related to the direction of the y axis
l	Related to the direction of the principal axis which has rotated θ degrees from the y axis direction

2      Related to the direction of the principal axis  
which has rotated  $\theta$  degrees from the x axis  
direction.

## ACKNOWLEDGEMENT

The author wishes to express his sincere gratitude to the staff of the Department of Aeronautics of the Naval Postgraduate School for their assistance in this project, with particular appreciation to Professor C. M. Smith for his guidance and advice throughout the period of this investigation and to Messrs. R. A. Besel and T. B. Dunton for their technical assistance.





## INTRODUCTION

The compact heat exchanger module concept has become increasingly more interesting as the scope of application of the gas turbine powerplant broadens.

One of the methods of raising the efficiency of the gas turbine so that turbine engines may compete economically with more conventional power plants is to recover a maximum amount of heat from the exhaust gas and use it to preheat the inlet air.

Since there are many sizes of gas turbine engines available, it would seem appropriate to design an efficient modular compact heat exchanger, thus allowing the addition of a specific number of modules to meet the requirements for a particular installation.

At least two studies were conducted for NAVSHIPSYSCOM in References 1 and 2; several designs were offered, and some were fabricated and tested. However, the anticipated service life of 20,000 to 60,000 hours was never approached. In fact, the longest service life of a test module to date is several hundred hours.

Several modes of failure for the compact heat exchanger have been proposed by Hamilton Standard (1) and Airesearch (2). Those failure modes which are a direct consequence of the shear lag deflection phenomenon are explained below.

One of these proposed failure modes is the failure of the parting sheet due to longitudinal cracks which develop as the result of shear stress induced by the temperature

differences between the parting sheet and closure bar. Another of the proposed failure modes is also concerned with shear lag, but this failure mode is manifested as longitudinal cracks in the closure bars. Shear lag deflections set up by the difference in temperature between any two adjacent parting sheets is considered to be the primary cause of this second mode of failure. Contributing to the second failure mode also is the shear lag in the normal direction to the closure bars which sets up bending deflections in the closure bars.

Several computer studies have been conducted, Hamilton Standard (1), Airesearch (2), and Corbett and Stubbs (3), utilizing assumed temperature distributions as the forcing function and extracting stress distributions which tend to verify the two modes of failure as proposed above. Hamilton Standard (1), Airesearch (2), and Kuhn (4) each offer the classical analytical solution to the shear distribution problem. That is, the shear stress level at any point along the parting sheet closure bar junction is described in terms of a decreasing exponential.

$$\tau = K P_0 e^{-ky}$$

The subtle variations in the definition of the parameters  $K$  and  $P_0$  are a result of the respective derivations.

The assumptions which were made in the course of the development of the respective proposals categorically

include: (1) The shear panel carries no tensile or compressive loads, and (2) no buckling occurs in the plane of the sheet. The assumption of a value for the effective-sheet-width was a matter of local preference. An effective-sheet-width of one and one-half inches, Reference 2, two times the width of the closure member in the direction of the sheet, Reference 1, and 40 per cent of the sheet width, Reference 5, was used in each respective analysis. Additionally, Lachman (5) assumed that: (1) All changes in lateral sheet dimensions due to the applied loading were small and therefore could be ignored; (2) superposition of loadings applied, and all load-deflection relationships were linear; and (3) all axial load carrying members were of constant cross section. The assumption of one dimensional heat flow was utilized in References 1 and 2 where the loading was a result of thermal shock.

Several additional assumptions were indicated in References 1 through 3 as necessary in order to achieve a numerical solution from available computer programs. Results thus obtained from existing theoretical analysis must be applied only to regions of the core which are remote from corners where one dimensional heat flow may be assumed to exist. The equations which were used to determine stress levels are valid only as order of magnitude expressions.

Two generally accepted solutions to the thermally induced shear lag deflection phenomena are (1) to balance

the mass distribution such that all components of the core; i.e., closure bars and parting sheets, will increase their respective temperatures at the same rate, and (2) to increase the time span of the ramp input function, that is, to restrict the hot flow cycle temperature increase to the same rate that the more massive core members are able to achieve.

Implementation of the above alternatives will undoubtedly render the shear lag deflection phenomenon an unimportant contributor to failure in the compact heat exchanger module. It is foreseeable, at least to this investigator, that, due to structural fabrication techniques, the mass distribution balancing solution would be unusable or at least undesirable. An additional restriction, such as hot cycle temperature rise time, may be undesirable from an operational point of view.

This study was undertaken to define the local stress concentrations and shear stress gradients which occur at the junction of the simulated closure bar and parting sheet.

It was also intended to derive some qualitative information which would help establish a working criterion for effective sheet width determinations.



## THE MODEL

It is fundamental to the technique of solving complicated problems that a suitable model be adopted, be it a mathematical model for an analytical solution or a mechanical model for an experimental solution. The suitability of such a model is a function of the reliability of the results which it yields, as well as a function of ease with which the model may be fabricated, employed, and instrumented. Raphael (6) lists considerations to be made in the selection of a structural model. Among these are geometric similarity, scale factor, boundary conditions, model and prototype relationships, joints, supports, test setup, and test procedure. Raphael (6) summarizes model and prototype relationships as shown in Table I. Other references concerning the choice of appropriate models are those by Heldenfels (7), Conrad (8), and Beggs, Davis and Davis (9).

It was within the guidelines above that the selection of a suitable model was accomplished to aid in the solution of the shear lag problem related to the compact heat exchanger project.

The models used in previous studies conducted by Hamilton Standard (1) and Airesearch (2) were evaluated and found to be insufficient in their ability to portray the complicated stress field in the closure bar parting sheet joint region.

Figure 1 illustrates the model employed by Hamilton Standard for use in conjunction with a computer study of

the transient temperature distribution and the resulting induced stress field at the closure bar parting sheet joint. The assumptions inherent in Figure 1 are such that lateral sheet compressive loads are not considered, and the induced bending stresses in the closure bar due to the constraint of the stiff exterior shell corner fabrication are not considered in combination with other existing stress phenomena.

Hence, in an effort to satisfy the requirement to accurately portray the complicated states of stress which exist, the following model configurations were selected: an axially loaded tensile specimen to indicate the characteristics of the pure shear stress field, Figure 2; an axially loaded specimen to indicate the interaction of adjacent shear stress field, Figure 3; and, an axially loaded specimen with induced transverse compressive loads to illustrate the complex state of combined stress in the parting sheet as a result of shear stress field and compressive stress field interaction, Figure 4.

The initial configuration, Figure 2, was a pure tensile specimen which would require the transfer of the load through the mechanism of shear and bond. The second model type, Figure 3, was used to indicate the interaction of adjacent stress fields induced through the shear transfer mechanism. The third model type, Figure 4, was utilized to indicate the influence of a compressive sheet load in conjunction with the existing shear lag phenomena.

The compressive stresses were introduced as a consequence of relatively high bending moments in the simulated closure bar.

It was decided to fabricate the series of models out of photoelastic material, Appendix A, and to employ the technique of photoelastic stress analysis to gain qualitative insight as to the resulting stress fields.



## EQUIPMENT AND PROCEDURE

Figure 5 shows the general arrangement of the fundamental equipment employed throughout this series of experiments. The polariscope as shown is a circular polariscope. The plane polariscope configuration, without quarter wave plates, was employed to determine the orientation of the principal axis system, from the isoclinic fringe patterns, Figure 6. The actual technique employed is described by Dally (10).

Whenever the circular polariscope configuration was employed, the two quarter wave plates were positioned such that their respective principal directions were mutually perpendicular. This latter condition will be referred to as "crossed" quarter wave plates.

To obtain the integral order fringe field,  $N_1$ ,  $N_2$ ,  $N_3$ ..., the polarizer axis and the analyzer axis were positioned such that their respective principal directions were mutually perpendicular; i.e., crossed. To obtain the half order fringe patterns,  $N_{1/2}$ ,  $N_{3/2}$ ,  $N_{5/2}$ ..., the respective axes of the polarizer and analyzer were paralleled. Table II shows an alternate arrangement of components of the polariscope. Theoretically, it is of little consequence which of the two available schemes is used to obtain the respective light or dark field. It is difficult to obtain a set of high quality quarter wave plates; but when the quarter wave plates are always crossed, any error that might be introduced by one of the quarter

wave plates which differs from  $\pi/2$  by an incremental amount  $\epsilon$  will be at least partially nullified by the succeeding quarter wave plate.

Both white light and monochromatic light were utilized as the light source for various stages in the testing program. Monochromatic light is advantageous in that the fringe patterns obtained show only the location of the tints-of-passage; they are black and white. In regions of high stress where resulting fringes are close together, the use of monochromatic light allows for more accurate identification of various fringes. In regions where the fringes were remote from the point of interest, the Tardy method of compensation as given in References 10 and 11 was employed.

The employment of white light as a light source yields a multicolored fringe pattern. Qualitative comparison of distribution patterns obtained from a series of tests is easily accomplished with the multicolored fringe patterns. This is especially true when the fringes are widely separated.

Each color appearing in a fringe pattern which results from using white light as a light source may be identified with a specific value of principal stress differences. Moreover, the order of occurrence of the respective colors is predictable. Therefore, it is only necessary to identify the color at any point; refer to Table III which identifies each color with an attendant level of principal strain difference (invariant for plane stress models), and then

calculate the level of principal stress difference at that point. Table III also includes the principal stress difference for the materials used in this series of experiments; these values are dependent upon the material constants of the specific photoelastic material in use.

The tensile load was applied to the model using the Dillon Tensile Testing Machine, Figure 5. The load adapters, Figure 7, were designed specifically for this test series. It was the intent to keep the number of special fixtures to a minimum. Simplicity in design and fabrication of necessary adapters was stressed.

From the standpoint of flexibility of employment and the ability to yield immediate results, it was decided to use the Polaroid Land Camera, Model 110A, with a close-up kit, as the primary photographic instrument.

A photographic record of test results is highly desirable when performing photoelastic stress analysis. The photograph provides a means of documenting the program progress as well as allowing the analyst to review the test results at a later date.

The first model type, Figure 2, conceived as a device for qualitative shear stress field study, was photographed at applied tensile loads of zero, 150 pounds, 250 pounds, and 400 pounds. White light was employed as the light source, and both light field and dark field photographs were obtained. An additional photograph was obtained using the monochromatic source light; the applied tensile load was 400 pounds.

The second model type, Figure 3, was initially photographed at applied loading of zero, 200 pounds, 300 pounds, and 400 pounds for preliminary model evaluation and qualitative study. Subsequently the model was re-photographed at loadings of 280 pounds and 350 pounds to establish the most convenient distribution pattern for further study. The 280 pound test load was the loading selected for the detailed study program of this model type. The distribution patterns resulting from 280 pounds appeared to photograph more accurately due to the color balance of the stress field and also produced fringe patterns in the simulated closure bars which were easily countable and identifiable. All previous photography on this model type had been accomplished using a white light source.

The further study of the interacting stress fields resulting from the applied loading of 280 pounds required a complete photographic record. The areas of interest were designated as those areas of the parting sheet that are adjacent to the closure bars and the closure bars. A complete set of color photographs, close-ups, was obtained of the local areas of interest with both light field and dark field. Additional black and white photographs were taken, Figures 8 and 9, using the monochromatic light source.

The orientation of the principal axis system was determined, Figure 6, using the techniques as outlined by Dally and Riley (10). Simultaneous rotation of the polarizer and analyzer of the plane polariscope, in increments of 5



degrees of arc through a total arc of 90 degrees, established the locus of points having constant angles of orientation for the principal axis system. Mechanically the isoclinic fringe patterns were traced from a ground glass screen at each 5 degrees rotation of the polariscope. One of the principal axes is always parallel to the axis of the polariscope wherever the isoclinic line appears.

The third model type, Figure 4, has been used thus far for a qualitative comparison study of the effects of high transverse sheet loads upon the induced shear stress patterns. The stress-difference patterns obtained with an applied loading of 280 pounds have been of most interest. The monochromatic light source was used and photographs taken at the 280 pound load condition.

All color photographs were obtained using Polarcolor Type 48 film. The photographs, Figures 8 and 9, were obtained on Polapan Type 52, 4 inch by 5 inch, sheet film. The exposure and developing parameters were determined in accordance with the manufacturer's recommendations.

It is considered that the photographs obtained using the techniques described in this portion of the report have been adequate for the purpose of documentation of the test series.

## DISCUSSION

The level of maximum shearing stress at discrete stations,  $y_i$ , along the junction between the sheet and bar of the model, Figure 3, was established from the experimental evidence. This stress level is plotted in Figures 10 and 11, for the left and right parting sheet-closure bar junctions respectively, and is labeled  $\tau_{\max}$ . To confirm the validity of  $\tau_{\max}$  it was necessary to account for total load that was transferred from each bar to the sheet.

Employing Figure 7, discrete values of  $\tau_{xy}$  were determined from the expression

$$\tau_{xy} = \tau_{\max} \sin 2\theta$$

and plotted in Figures 10 and 11. Graphical integration of  $\tau_{xy}$  times the thickness over the length of the left and right closure bars indicated that 94.6 pounds and 95.4 pounds of the total load were transferred through the mechanism of shear at the respective closure bar-parting sheet junctions.

Appendix C discusses the determination of that portion of the applied load which is transferred as tensile stress from the ends of the closure bars. It was found that 55.5 pounds were transferred from the left bar and 54.6 pounds from the right bar through tension. The totals of the derived transferred loads is 7.2 per cent above the applied load of 280 pounds. It is concluded that the stress

distribution  $\tau_{\max}$ , as shown in Figures 10 and 11, is a valid interpretation of the photoelastic data.

The comparison of the experimentally derived  $\tau_{\max}$  curve to the predicted  $\tau_{\max}$  curves from References 1 and 2 will be limited to that portion which is within the region of interest as indicated Figure 12. It is assumed that the "region of interest" is not influenced by the stress concentrations induced by the discontinuity at the end of the closure bar.

The shear stress distribution in the sheet, as shown in Figures 10 and 11, for  $y$  between zero and one half is explained qualitatively by Kuhn (4). The peak value of shearing stress in a sheet is known to be related to the rigidity of edge of the sheet along the  $y$  equals zero station. Figures 10 and 11 indicate no departure from the expected shear stress distribution for the condition of zero restraint at the  $y$  equals zero boundary. Likewise, an increase in stiffness along the  $y$  equals zero boundary will require a corresponding increase in the peak value of shear stress. Extrapolation of the experimentally obtained curve in the manner indicated, Figure 12, is supported by Kuhn (4) and is considered justified for the limiting case of an infinitely rigid restraint along the  $y$  equals zero edge of the sheet.

Figure 12 is a comparison of the experimentally obtained shear stress distribution with the predicted shear stress levels as predicted by References 1 and 2.

Throughout the calculations performed in the preparation of Figure 12, the material constants employed were those which characterized the plastic material utilized in model construction, Table IV. The effective sheet width employed in the calculations was determined by using the criteria as established in References 1 and 2 for their respective proposals.

$\tau_{ave}$  as it appears in Figure 12 is the ratio of the total load transferred through the shear mechanism to the area of the first 3 inches in the  $y$  direction along the shearing surface.  $\tau_{ave}$  for this model versus load configuration was determined to be nominally 267 pounds.

The experimentally obtained distribution curve is observed to be at least 100 psi above the values predicted by References 1 and 2 over the entire region of interest. The maximum extrapolated shear stress is 14.9 per cent higher than the value predicted by Reference 2 and 23.9 per cent higher than the value predicted by Reference 1.

The occurrence of the high level shear stress distributions as a result of thermal shock is accompanied by: (1) shear lag deflection phenomena, (2) stress concentrations due to closure bar discontinuities and in-the-corner inclusions which occur at the joint of the manifold ducting to the heat exchanger core, (3) transverse bending stresses in the sheet induced by rigid exterior module case, (4) compressive stresses in the sheet induced by transverse expansion of the sheet which results from the thermal environment



of the module and the restraint of the rigid exterior module case, and (5) stresses which result from thermal gradients in the core due to blockage or fouling.

The uncertainty involved in the prediction of stress levels at any point in the heat exchanger module is obvious.

Techniques which so far have been unable to account for the complicated states of stress present in the closure bar-parting sheet junction region, as evidenced by failure of prototype models, must be reviewed as to the probability of obtaining worthwhile results. The fact that the actual stress level is generally above the predicted value is no surprise. The load function of the predicted curves could easily be in error by as much as 30 per cent as was discussed earlier. Perhaps the problem is not the analytical technique but rather the accurate prediction of the load function. In any case, the result is the same, a level of predicted stress significantly below the actual level.

It is proposed here, that for the purpose of the designer, the assumption of a linear shear stress distribution with a maximum shear value of  $2.5 \tau_{ave}$  is not unrealistic for the case at hand. It may be that the maximum predicted values of  $\tau_{max}$  by References 1 and 2 may be improved by a nominal factor ranging to 30 per cent above the maximum predicted value to obtain a realistic  $\tau_{max}$ .

It is acknowledged that the arbitrary adoption of certain parameters in the selection of a model, specifically with respect to sheet thickness, bar length, bond of

bar to sheet and geometric relationship of the various parts, limits somewhat the usefulness of the above model. But it is expected that the results obtained from the tests conducted are indicative of the occurrence of stress levels above the predicted level when the inherent assumptions are no longer valid.

The qualitative comparison of the photoelastic patterns of  $\tau_{\max}$  shows that the distribution pattern of model type Figure 3 is not an isolated situation. Figures 8, 9, 13, 14, 15, and 16 illustrate the various  $\tau_{\max}$  distributions that were obtained. Indeed, the similarity between stress distribution patterns of the various model types was reassuring.

The high lateral compressive loads, induced in the sheet by the loading mechanism of model Figure 4, had the effect of increasing the level of the maximum shear value at the sheet edge,  $y$  equals zero boundary. The comparison was conducted qualitatively, but the increase in shear stress level was remarkably obvious.

Although only a limited amount of data was gathered, it is believed that the results shown herein are indicative of the need for simple models, as pointed out by Smith (13), from which to gather design information. Prototype testing, especially when the size of the prototype is small, has proven to be impractical. The compact heat exchanger module is a good example.

## CONCLUSIONS AND RECOMMENDATIONS

The following conclusions are based on the photo-elastic model study of the closure bar parting sheet joint region of a compact heat exchanger module. Recommendations are included where appropriate.

1. Present methods of predicting the maximum shear stress levels are inadequate when applied to the heat exchanger module. It is believed that increasing the predicted values of shear stress by a nominal factor of 30 per cent is reasonable to account for the complicated stress state which exists in the critical regions of the parting sheet.
2. Extrapolation of the experimentally obtained stress distribution curve Figure 12 is valid. It might be worth-while to investigate the degree of stiffening along the  $y$  equals zero boundary necessary to raise the maximum stress values, Reference 4.
3. Increased longitudinal sheet edge flexibility will substantially reduce the maximum induced shear values resulting from thermal shock environment. This conclusion is supported by Kuhn (4).
4. For the purpose of engineering design the determination of a maximum shear stress value may be calculated as approximately 2.6 times  $\tau_{ave}$ . The accompanying distribution pattern may then be considered to vary

linearly along the length of the closure member. The apparent crudeness of this proposal may be justified by acknowledging the complicated states of stress which exist and the present inability to adequately cope with these situations in the design of the heat exchanger module. The predicted maximum stress is essentially independent of the length of the closure member. By defining  $\bar{T}_{ave}$  over the first 3 inches of the closure bar, any modification in length will not cause difficulty.

5. The arbitrary selection of certain model parameters is somewhat restrictive as to the scope of application of the results of this experiment.
6. Qualitative analysis of various model configurations is useful in establishing stress distribution patterns, and it allows the investigator to determine relative maximum stress levels rapidly.
7. The technique of photoelastic stress analysis lends itself well to qualitative study; and, with little added effort, a quantitative determination of stress levels may be accurately accomplished. It is necessary to obtain quantitative information from selected distribution patterns only. The photoelastic display then allows for visual comparison of the states of stress present in a given series of models.



## BIBLIOGRAPHY

1. Hamilton Standard (Division of United Aircraft Corporation), Windsor Locks, Connecticut, Thermal Stress and Transient Behavior and Thermal Fatigue Criteria for Marine Recuperators. Quarterly Progress Report, Period 1 January to 31 March 1967 - SP6782, Contract No. NOBS-92558, Naval Ship Systems Command.
2. Airesearch Manufacturing Division (Garrett Corporation), Los Angeles, California, "Exhaust Gas to Compressed Air Recuperator Base Load Gas Turbine Study." Edited by E. F. Bush. Report L-9406, 1 April 1964.
3. Corbett, R. L. and Stubbs, D. W., "An Investigation of the Pressure Stresses in a Compact, Plate Fin, Counterflow Heat Exchanger." Unpublished Master's thesis, Naval Postgraduate School, Monterey, California, 1966.
4. Kuhn, Paul and Peterson, James, P., Shear Lag in Axially Loaded Panels, Technical Note No. 1728. National Advisory Committee for Aeronautics, October 1948.
5. Lachman, Richard H. and Schweitzer, Vance A., "Investigation of Shear Lag in Panels With and Without Cutouts." Unpublished Master's thesis, University of Michigan, Ann Arbor, Michigan, May 1950.
6. Raphael, Coleman, "Considerations in the Design of Structural Models," Aeronautical Engineering Review, Vol. 14, February 1955, pp. 52-55.

7. Heldenfels, R. R., "Models and Analogs," High Temperature Effects in Aircraft Structures. Edited by John Hoff Nicholar. Published for AGARD by Pergamon Press, 1958.
8. Conrad, R. D., Structural Models Part 1: Theory, C and R Bulletin No. 13, Navy Department. U. S. Government Printing Office, June 18, 1938.
9. Beggs, George E.; Davis, Raymond E.; and Davis, Hammer E., Tests on Structural Models of Proposed San Francisco-Oakland Suspension Bridge. University of California Press, Berkeley, California, 1933.
10. Dally, J. W. and Riley, W. F., Experimental Stress Analysis. New York: McGraw Hill Book Company, Inc., 1965.
11. Tuppeny Jr., W. H. and Kobayashi, A. S., Manual on Experimental Stress Analysis, Second Edition, Society for Experimental Stress Analysis, 1965.
12. Zandman, Felix, "Photoelastic-coating Tests," Nondestructive Testing Handbook, Vol. II, Society for Nondestructive Testing, New York: The Ronald Press Company, 1959.
13. Smith, Cameron M., "Experimental Stress Investigation," Annual Research Report - Studies of Thermal Stress in Heat Exchanger (Naval Ships System Command - Code 0645). Phase of Gas Turbine Regenerator Fouling Investigation. Period 1 July 1966 to 30 June 1967 and 1 July 1967 to 10 November 1967. Naval Postgraduate School, Monterey, California. (Unpublished)

## APPENDIX A

### FABRICATION OF THE MODELS

It was realized that in general the mixing of types of various model building materials in the fabrication of a model was to be avoided; however, due to the unavailability of a range of thicknesses of any one type of material sufficient to cover the needs of the experiment, the alternative of using material from more than one batch, and further from more than one supplier, was considered and accepted.

A consequence of the above decision was the resultant high stress-optic-coefficient,  $C$ , of the 0.120 inch thick material, coincident with the low order fringes in the simulated parting sheet, obtained from the applied loadings.

The bonding of the respective pieces of each model type was accomplished with minimum variation in bonding agent mixing and in application techniques.

The bonding of parts on the top surface of the sheet was performed at which time the bonding agent was allowed to cure for a period in excess of 12 hours at room temperature. The model was then turned over, and the bonding was again performed on the top surface, allowing a similar length of time for curing.

All pieces were thoroughly cleansed with acetone before the application of the bonding agents. In all cases, the resin-hardener mix was a 10:1 ratio by weight, as is recommended by the supplier. After a thorough mixing period of

3-5 minutes, the resin-hardener mixture was allowed to stand for a period of 10-15 minutes before application. The recommended pot life of the bonding agent is 20-25 minutes. This length of time was more than adequate to allow for positioning and alignment of the various components prior to set.

All raw edges (edges which had been machined) were then coated with a thin application of the bonding agent. This sealed the model against the absorption of moisture, thus preventing time edge effects from ruining the model.

Table IV indicates the particular materials that were used to fabricate the respective model types. All model materials were a product of Photolastic Inc., except that the Type S material is a product of the Photostress Company.



## APPENDIX B

### PHOTOELASTIC CALIBRATION OF BUILT-UP LAMINA AS EMPLOYED IN SIMULATED CLOSURE BAR CONSTRUCTION

A tensile test specimen was constructed by bonding a sheet of PSM5 material on each side of a sheet of PS2A material, Tables IV and V, in accordance with the procedure outlined in Appendix A.

The width,  $w$ , and thickness,  $h$ , of the test specimen were measured and found to be:

$$w = 0.980 \pm .002$$

$$h = 0.630 \pm .002$$

From the basic linear stress relationship,

$$\sigma = \frac{P}{A}$$

where:  $P$  = applied tensile load and

$A$  = cross sectional area of test section

The calibration curve was calculated and plotted.

The test specimen was then placed in the Dillon testing machine. The magnitude of the applied load was noted and recorded at each tint of passage, Table VII.

The value of  $N$  for each tint of passage was then established. A simple averaging procedure resulted in a

stress optic constant, C, of 56.7 psi. per fringe per inch.

Sample calculations for Appendix B were:

$$A = hw = .630 \times .980 = .616 \text{ sq in}$$

$$\sigma_x = \frac{P_x}{A} = \frac{100 \text{ lbs}}{.616 \text{ sq in}} = 162 \text{ psi}$$

$$C = \frac{1}{n} \left[ \sum_{i=1}^n \frac{\sigma_{N_i}}{i} \right] t$$
$$= \frac{1}{4} \left[ \frac{81}{1} + \frac{178}{2} + \frac{278}{3} + \frac{381}{4} \right] (.63)$$

$$C = 56.7 \text{ psi/fringe/in}$$

## APPENDIX C

### DETERMINATION OF THE PORTION OF THE LOAD TRANSMITTED AS TENSION

The value of  $\sigma_1 - \sigma_2$  was established at discrete points along the edge,  $y = 3$ , of the respective simulated closure bars. The principal axis orientation is shown in Figure 6. At the free edge

$$\sigma_x = \sigma_y = 0 ; \quad \theta = 0$$

and from Mohr's circle

$$\sigma_y - \sigma_x = (\sigma_1 - \sigma_2) \cos 2\theta$$

It is assumed that  $\sigma_x = 0$  everywhere along the edge of the closure bar at  $y = 3$ .

Hence a value for  $\sigma_y$  may be determined across the bottom of the bar at a discrete number of locations. That portion of the applied load which is transferred to the sheet as a tensile stress is determined from

$$P_{\text{tensile}} = \sum_{i=1}^n (\sigma_y \cdot \Delta x)_i t_i$$

and found to be 55.5 pounds and 54.6 pounds for the left and right closure bars respectively.

The combination of these loads with the load transferred through shear shows a difference of 7 per cent from the applied load of 280 pounds.

To further justify the established levels of tensile stress, consider the situation where the fringe value everywhere along the bottom edge of both bars is  $N_{3/2}$ ; the maximum value of end load would then be

$$(t) \ (w) \ (\sigma_1 - \sigma_2) = 61 \text{ lbs/closure bar}$$

This would correspond to a disagreement with the input load by 11.4 per cent. This value is arrived at using the conservative assumption that  $\theta = 0$ ; it may therefore be considered a limiting situation.

A finite difference approximation scheme could have been used to determine the value of  $\sigma_y$  at various stations. The computational time that would have been necessary was not considered justifiable. The computational errors are also cumulative necessitating a high degree of certainty of all input data.

TABLE I  
SUMMARY - MODEL / PROTOTYPE RELATIONSHIP

Type I - Structural similarity  
 Type II - Geometric similarity  
 Type III - Prototype & model mat'l the same

	Type I	Type II	Type III	(Geom. sim.) Type IV
Bending deflections	$N_L$	$N_L$	$N_L$	$N_L$
Torsional angular deflections	1	1	1	1
Bending and twisting moments	$N_F N_L$	$N_L^3$	$N_L^3$	$N_L^3$
Axial stresses	$\frac{N_F}{N_L^2}$	1	1	1
Bending stresses	$\frac{E_P}{E_M} \frac{c_P}{c_M} \frac{1}{N_L}$	$\frac{E_P}{E_M} \frac{c_P}{c_M} \frac{1}{N_L}$	$\frac{c_P}{c_M} \frac{1}{N_L}$	1
Torsional shear flow	$\frac{q_P}{q_M}$	$\frac{A_M}{A_P} N_F N_L$	$\frac{A_M}{A_P} N_L^3$	$N_L$

SYMBOLS

A = area, sq.in.  
 c = distance - bending axis to extreme fiber, in.  
 E = modulus of elasticity, lbs/sq.in.  
 G = modulus of rigidity, lbs/sq.in.  
 I = rectangular moment of inertia, in.<sup>4</sup>  
 J = polar moment of inertia, in.<sup>4</sup>  
 k = spring constant of supports  
 K = any constant  
 L = length, in.  
 M = bending moment, in.lbs.  
 N<sub>L</sub> = prototype/model length.  
 N<sub>F</sub> = prototype/model forces.  
 P = load, lbs.  
 q = shear flow, lbs/in.  
 s = stress, lbs/sq.in.  
 T = torque, in.lbs.  
 Δ = linear deformation or deflection, in.  
 θ = angular deformation or deflection, rad.  
 P = prototype  
 M = model

SUBSCRIPTS

TABLE II

FOUR ARRANGEMENTS OF THE OPTICAL ELEMENTS IN A CIRCULAR POLARISCOPE

Arrangement	Quarter Wave Plates	Polarizer and Analyzer	Field	Field Order
A *	Crossed	Crossed	Dark	Integral
B *	Crossed	Parallel	Light	Half
C	Parallel	Crossed	Light	Half
D	Parallel	Parallel	Dark	Integral

\*Preferred



TABLE III  
PHOTOELASTIC COLOR STRESS CONVERSION

Dark Field (Crossed)	Light Field (Parallel)	Type S		PS-2	
		$\epsilon_1 - \epsilon_2$ ( $\mu$ in/in)	$\sigma_1 - \sigma_2$ (psi)	$\epsilon_1 - \epsilon_2$ ( $\mu$ in/in)	$\sigma_1 - \sigma_2$ (psi)
N <sub>0</sub> Black	White N <sub>0</sub>	0	0	0	0
Grey	Yellowish-white	370	122.4	279	92.3
White	Light Red	935	309.4	705	233.3
Very pale yellow	Dark Red Brown	1000	330.8	754	249.5
-	N <sub>1/2</sub>	1021	337.8	770	254.8
Bright Yellow	Indigo	1087	359.7	820	271.3
Brown-Yellow	Gray-Blue	1565	517.8	1180	390.4
Reddish-Orange	Bluish Green	1826	609.2	1377	455.6
Red	Pale Green	1956	647.2	1475	488
N <sub>1</sub>	-	2042	675.7	1540	509.6
Indigo	Gold-Yellow	2130	704.8	1607	531.7
Blue	Orange	2391	791.1	1803	596.5
Green	Red	2717	899	2049	677.9
-	N <sub>3/2</sub>	3063	1013.5	2310	764
Greenish Yellow	Violet	3152	1043	2377	786.5
Pure Yellow	Indigo	3304	1093	2492	824.5
Orange	Greenish-blue	3630	1201	2738	906
Dark Red	Green	3978	1316	3000	992.6

TABLE III (Cont'd)  
PHOTOELASTIC COLOR STRESS CONVERSION

Dark Field (Crossed)	Light Field (Parallel)	Type S		PS-2	
		$\epsilon_1 - \epsilon_2$ ( in/in)	$\sigma_1 - \sigma_2$ (psi)	$\epsilon_1 - \epsilon_2$ ( in/in)	$\sigma_1 - \sigma_2$ (psi)
N <sub>2</sub>	-	4084	1351	3080	1019
Indigo	Gray-Yellow	4152	1374	3131	1036
Green	Brown-Red	4782	1582	3606	1193
-	N <sub>5/2</sub>	5105	1689	3850	1274
Greenish-Yellow	Grayish-Indigo	5174	1712	3901	1291
Carmine Red	Green	5543	1834	4180	1383
N <sub>3</sub>	-	6126	2027	4620	1528
Green	Pale-Pink	6304	2085	4754	1573

TABLE IV  
MODEL MATERIALS

Model Type	Ref	Component		Resin Hardener
		Closure Bar	Parting Sheet	
I	Fig. 2	PSM5	PS2-A	PC1C PCH1
II	Fig. 3	PSM5	Type S	PC1C PCH1
III	Fig. 4	PSM5	Type S	PC1C PCH1

TABLE V  
MECHANICAL PROPERTIES OF PHOTOELASTIC MATERIALS

Material	C stress optic const (psi/fringe/inch)	E (1000 psi)	Poissons Ratio	Nomi- nal Thick- ness
PSM-5*	60	450	.36	.250
PS2-A*	510	450	.36	.120
Type S**	675	450	.36	.120
PC1C* PCH-1*	Resin Hardener	Bonding agent recommended for use with PS-2 material.		

\* Photolastic  
\*\* Photo Stress Co.

TABLE VI  
LIST OF EQUIPMENT

List of Equipment		
Polariscope		
Dillon Testing Machine	# 3796	
Dynamometer	# 3796-1	
Polaroid Land Camera	Model 110A # P 140 261	
Beaded Viewing Screen		
Ground Glass Reverse Viewing Screen		

TABLE VII  
CALIBRATION OF MATERIAL

Occurrence of Tint	Trial I	Trial II	$\sigma_1 - \sigma_2$
$N_1$		50	81
$N_2$	110	110	178
$N_3$	170	170	278
$N_4$	235	230	381
$\sigma_1 - \sigma_2 = \frac{CN}{t}$			
$C = 56.7 \text{ psi/fr/in}$			

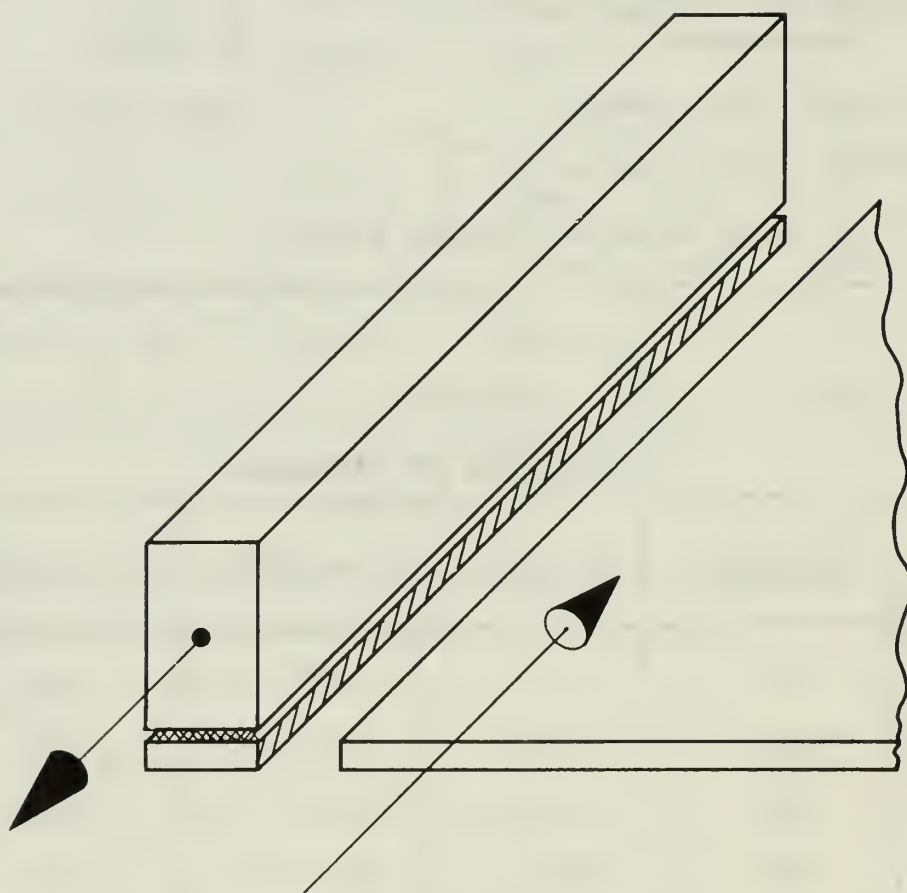


FIGURE 1  
IDEALIZED SHEAR LAG MODEL

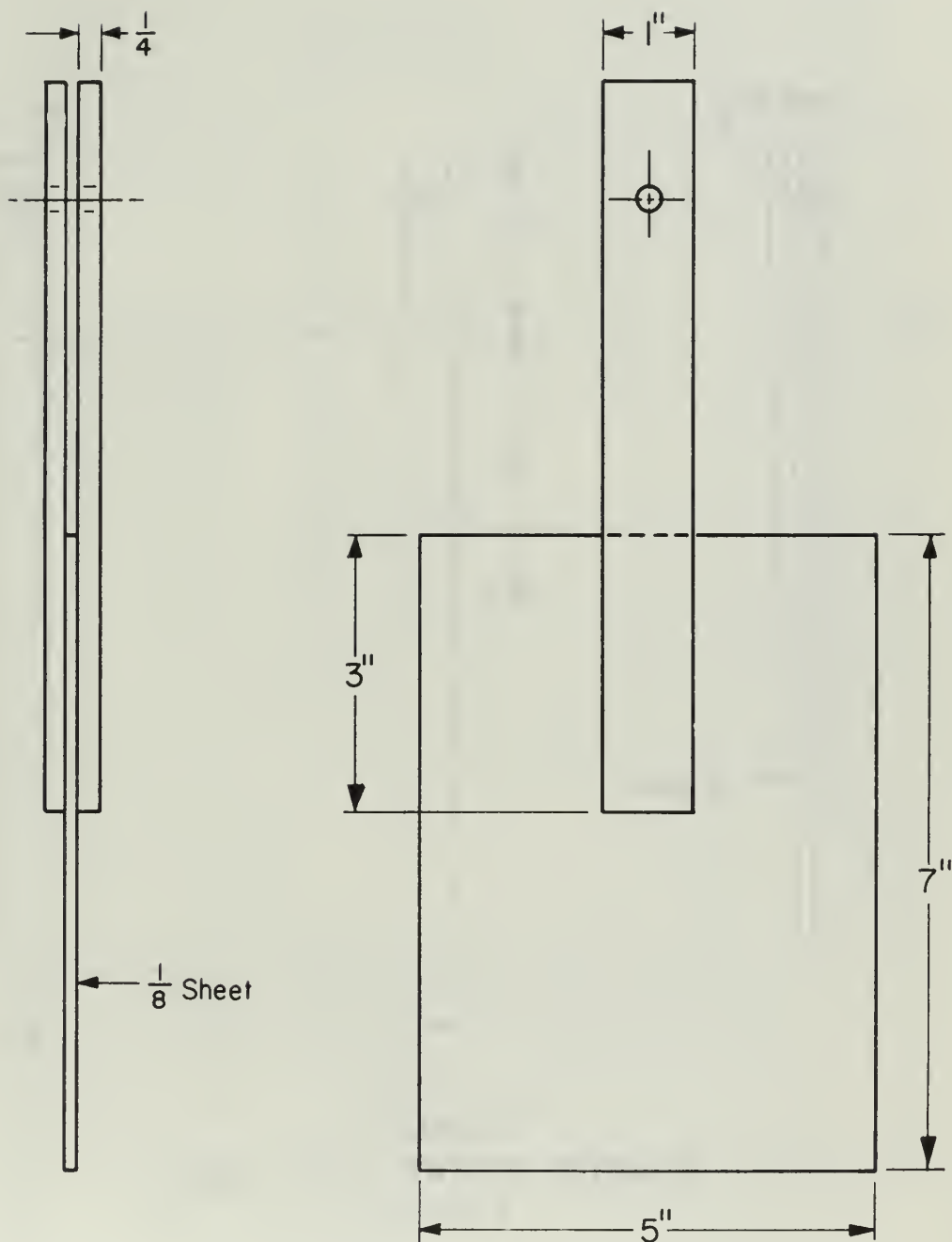


FIGURE 2  
PLASTIC SHEAR LAG MODEL  
TYPE I



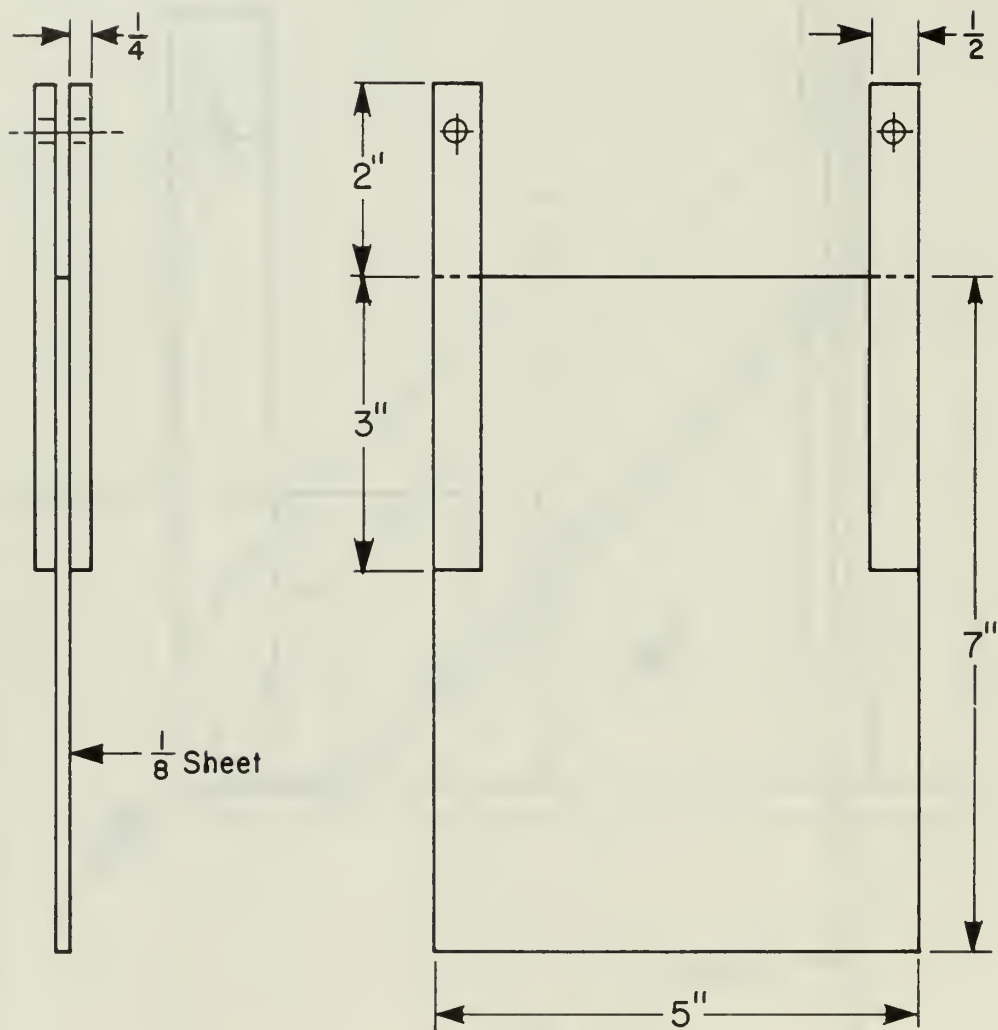


FIGURE 3  
PLASTIC SHEAR LAG MODEL  
TYPE 2

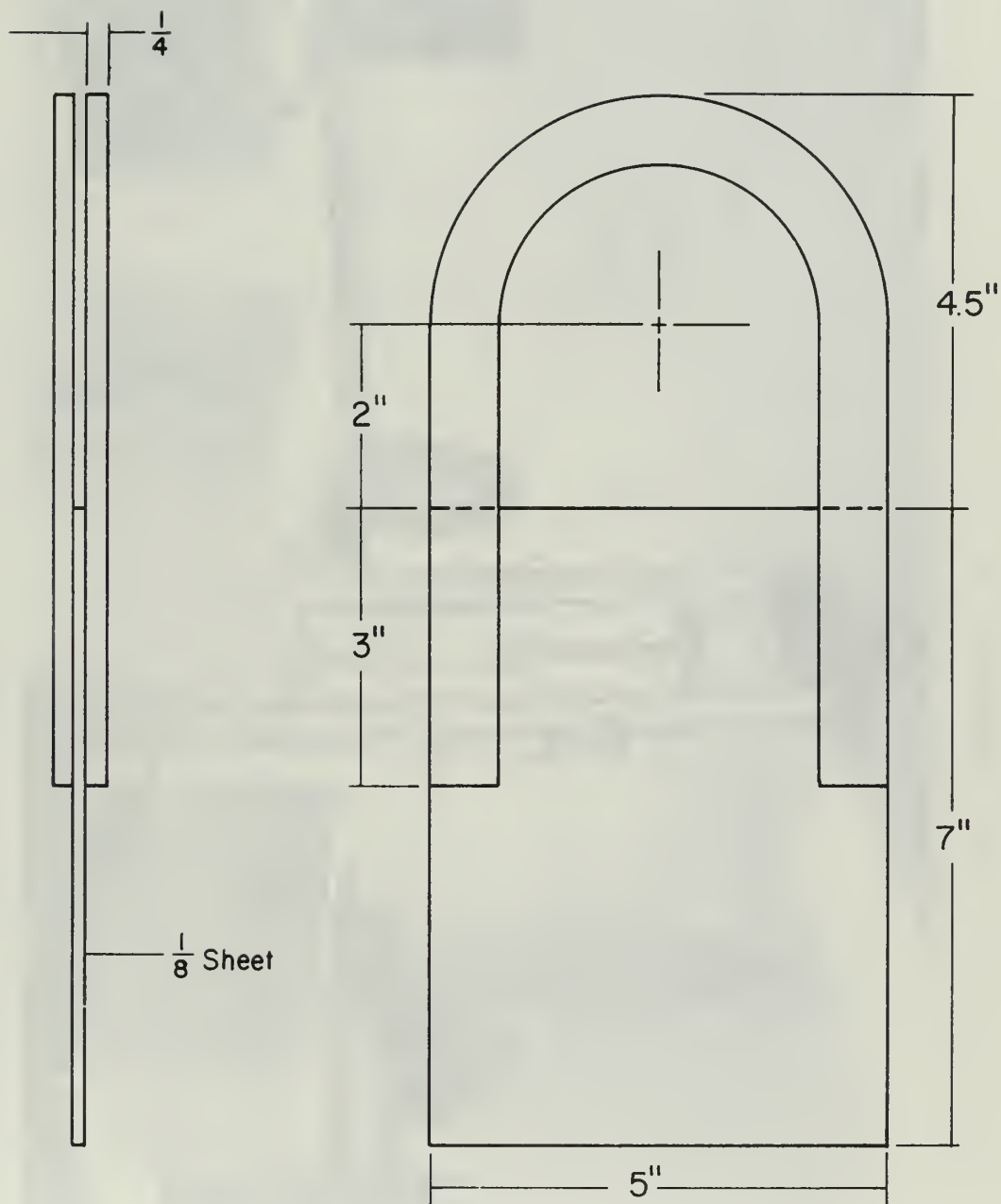


FIGURE 4  
 PLASTIC SHEAR LAG MODEL  
 TYPE 3

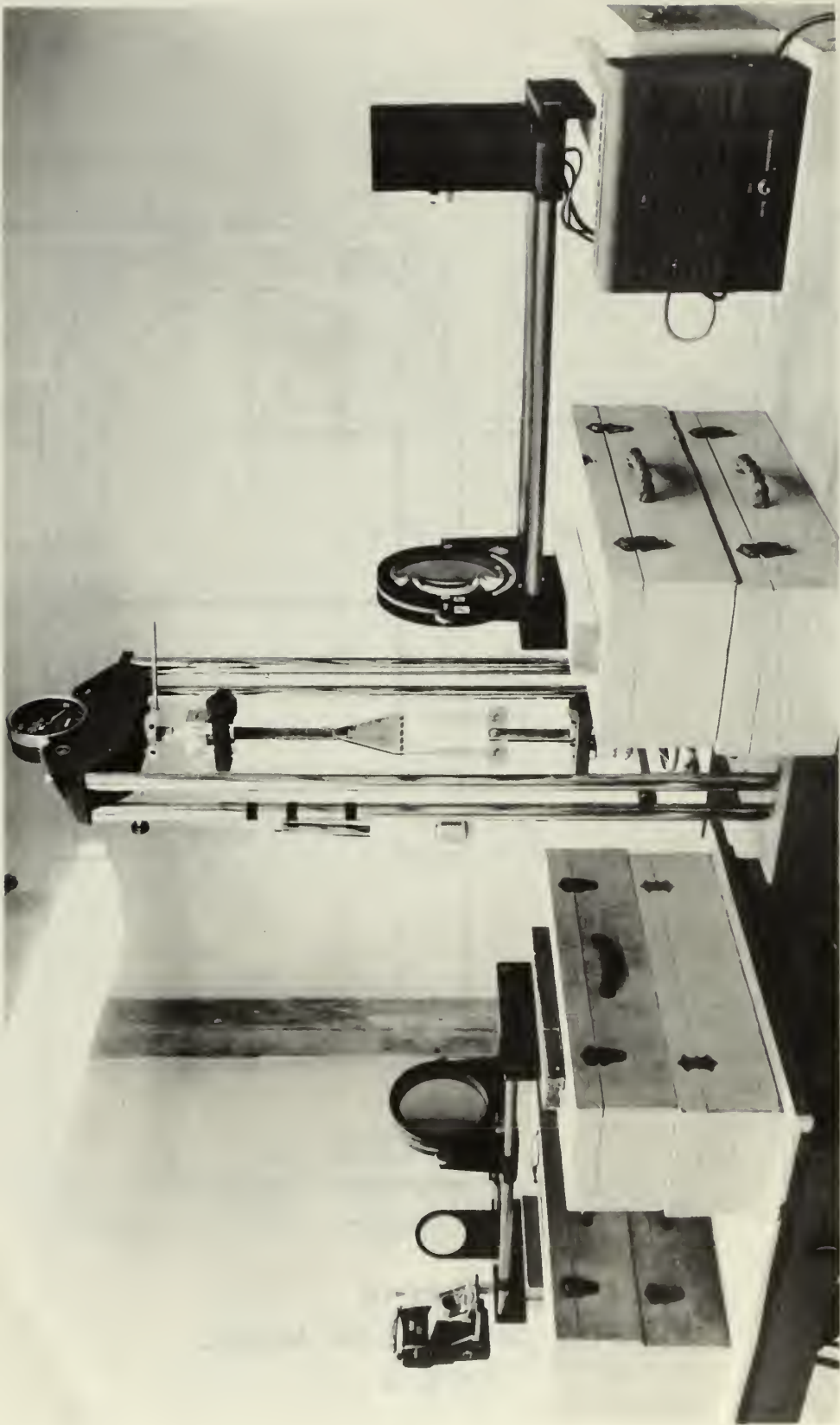


FIGURE 5  
EXPERIMENTAL SETUP

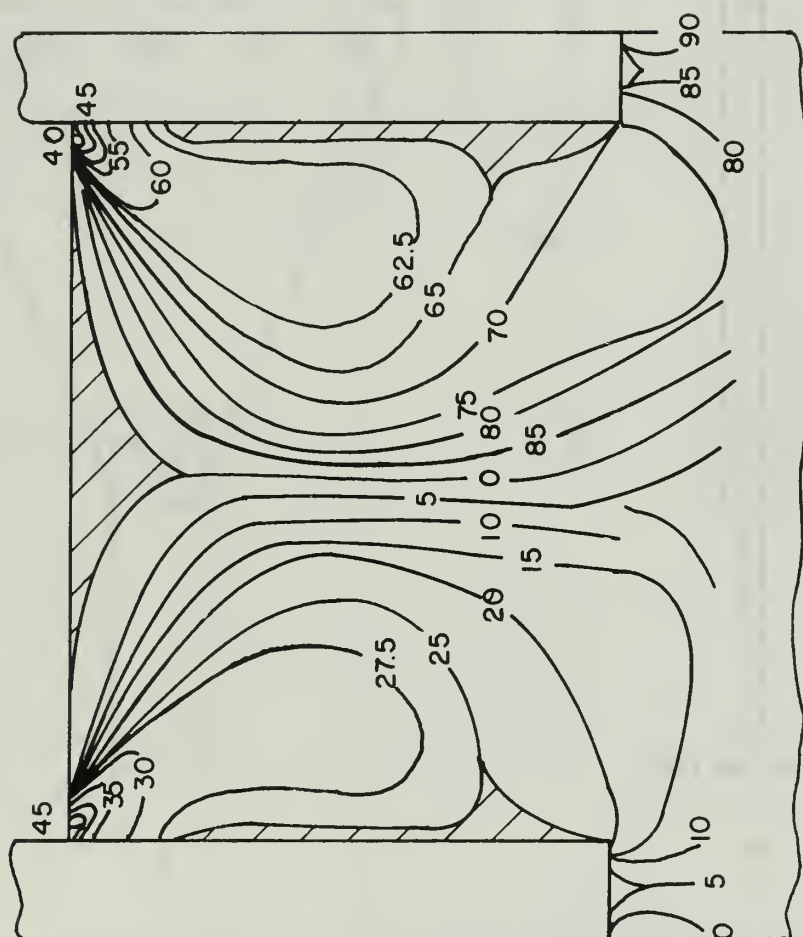


FIGURE 6  
PRINCIPLE AXIS ORIENTATION CONTOURS  
OF CONSTANT  $\theta$

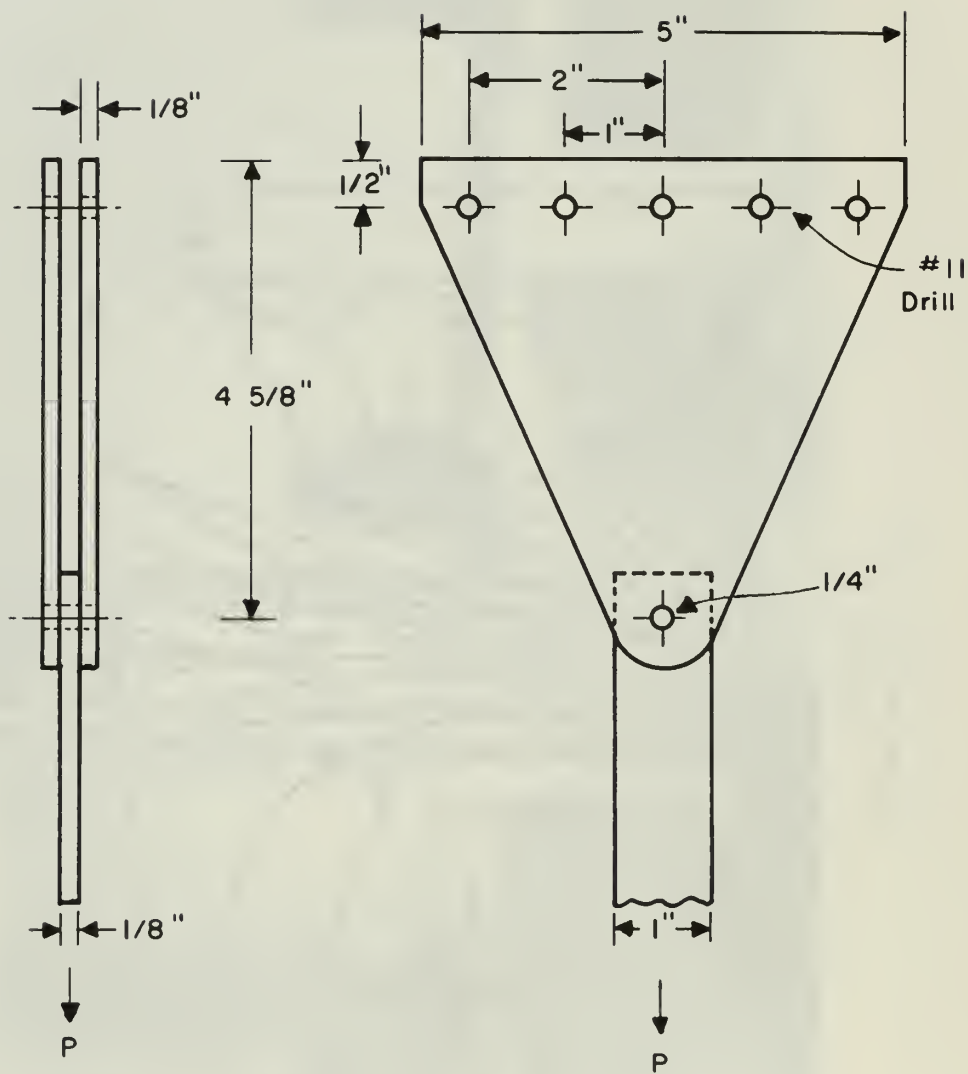


FIGURE 7  
MODEL LOAD ADDAPTER



FIGURE 8  
INTEGRAL ORDER FRINGE PATTERN MODEL TYPE 2



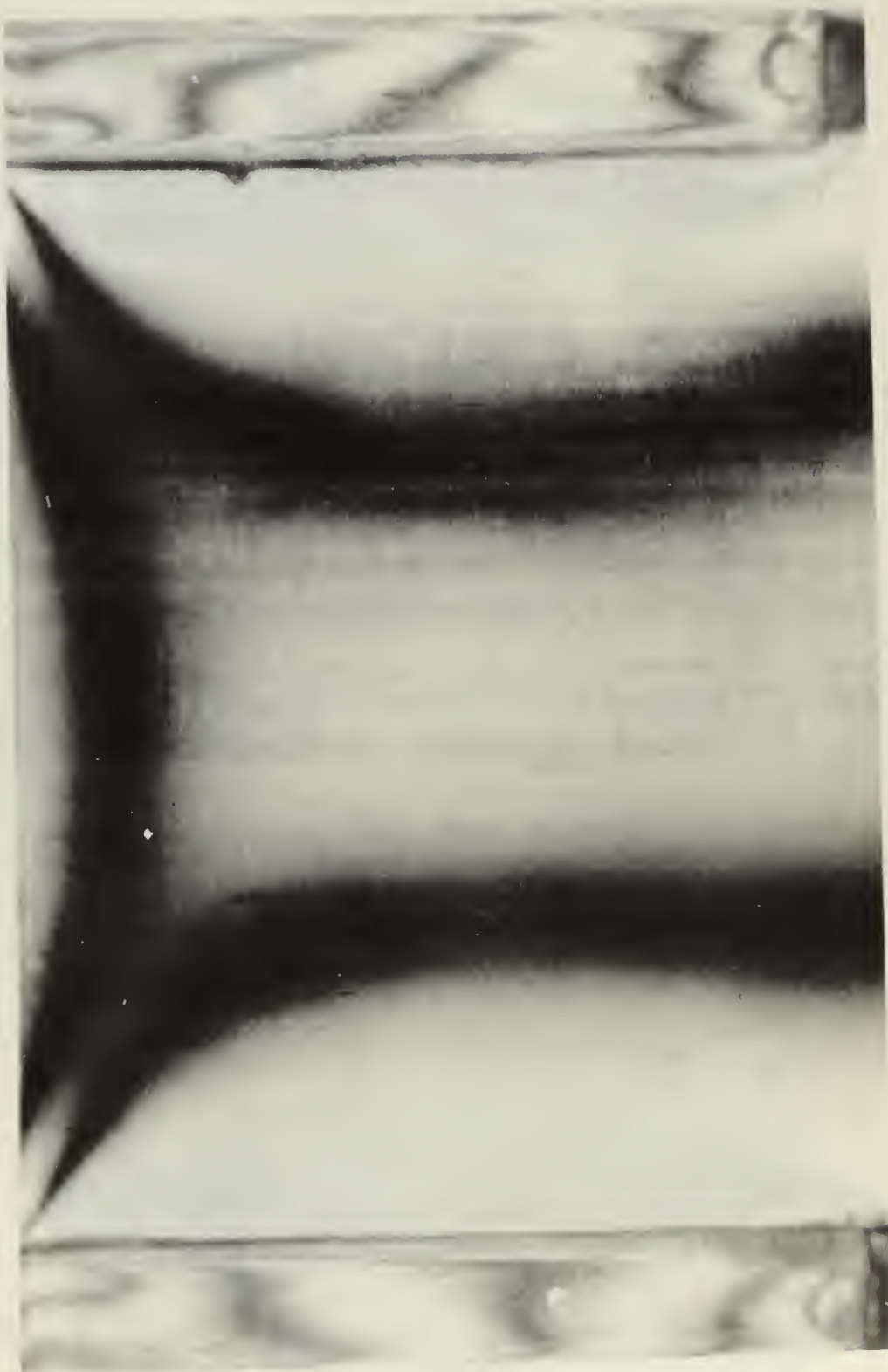


FIGURE 9  
HALF ORDER FRINGE PATTERN MODEL TYPE 2

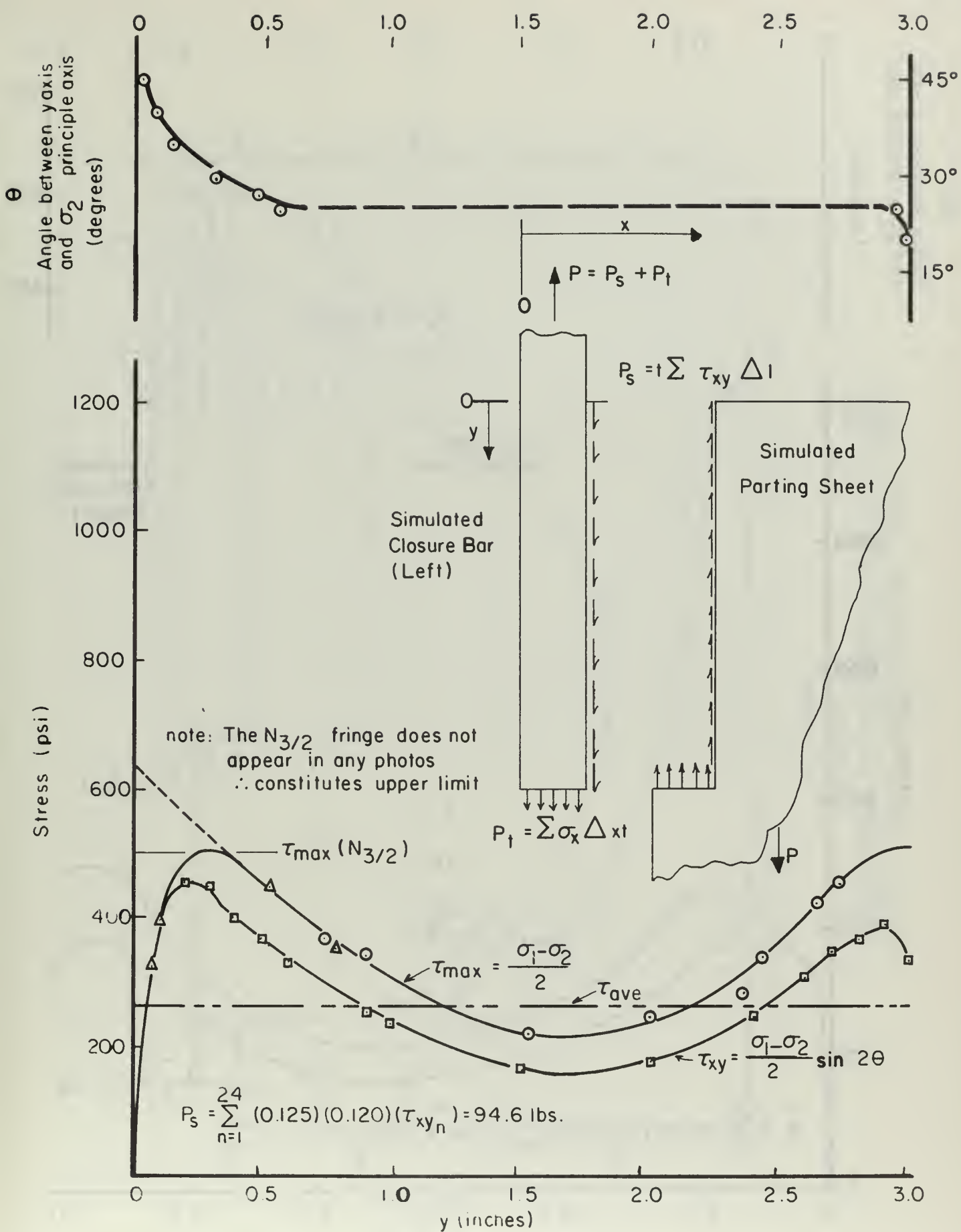


FIGURE 10  
SHEAR DISTRIBUTION IN SHEET  
ALONG LEFT CLOSURE BAR

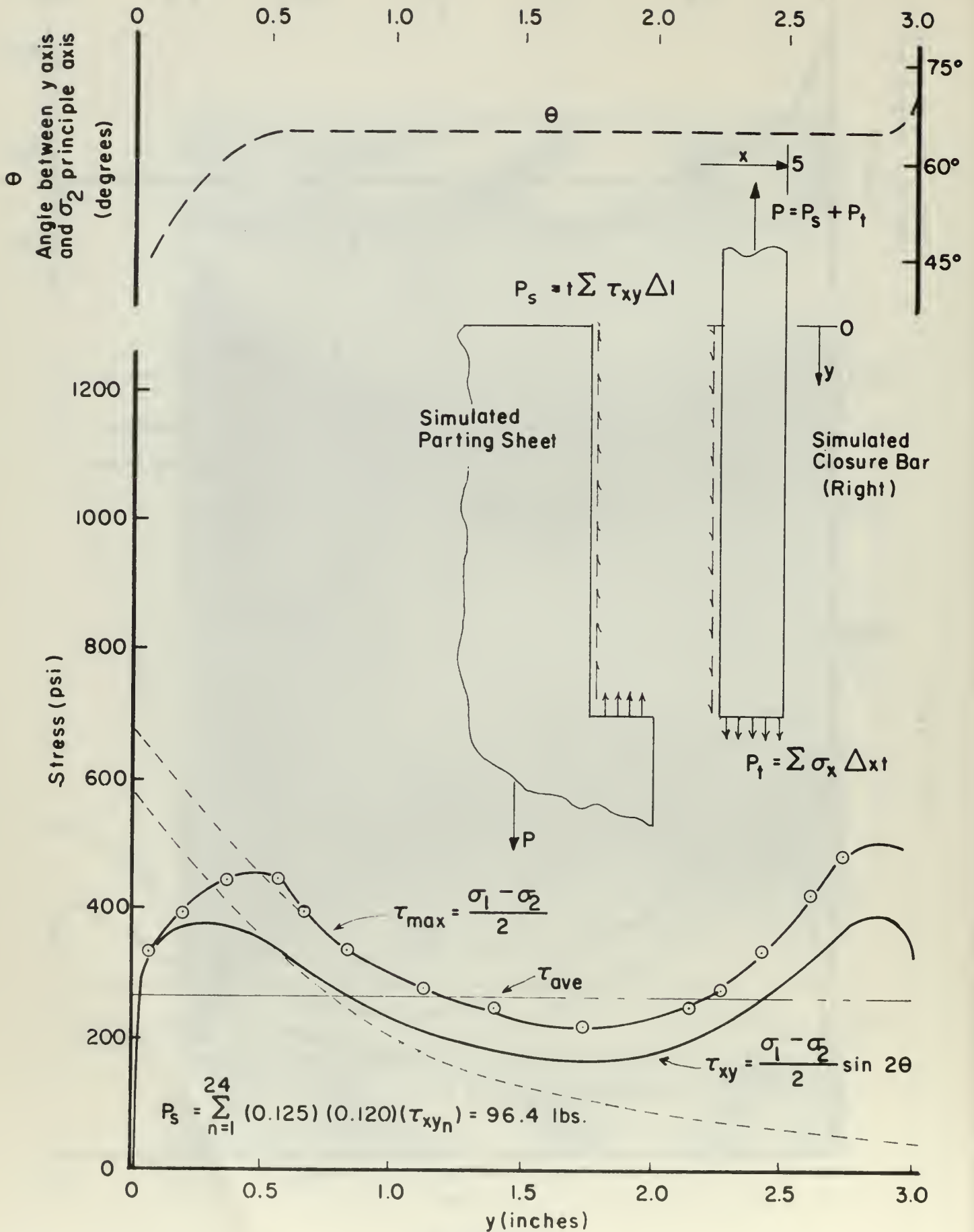


FIGURE II  
SHEAR DISTRIBUTION IN SHEET ALONG  
RIGHT CLOSURE BAR

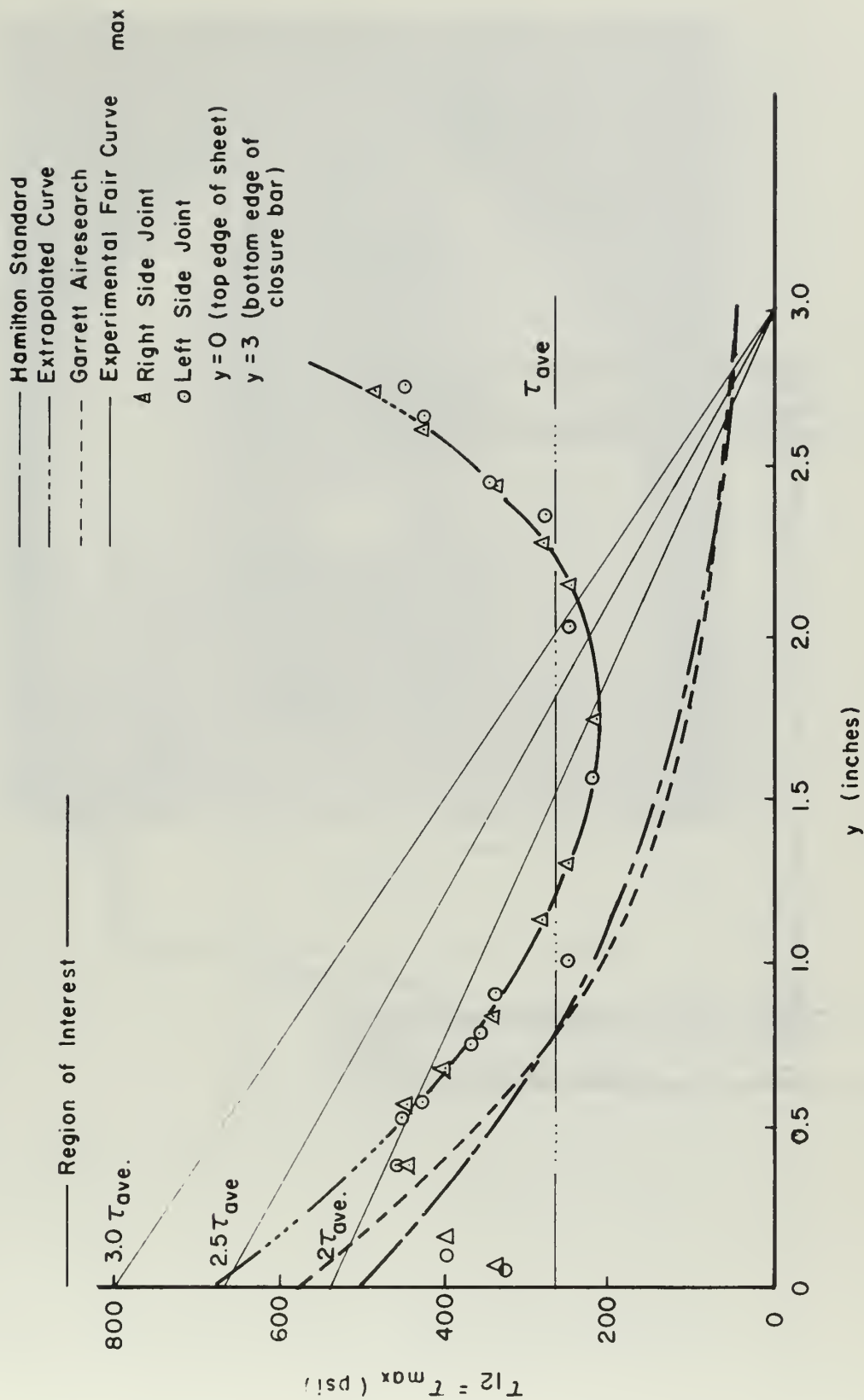


FIGURE 12  
 COMPARISON OF PREDICTED SHEAR STRESS  
 LEVELS WITH EXPERIMENTAL RESULTS

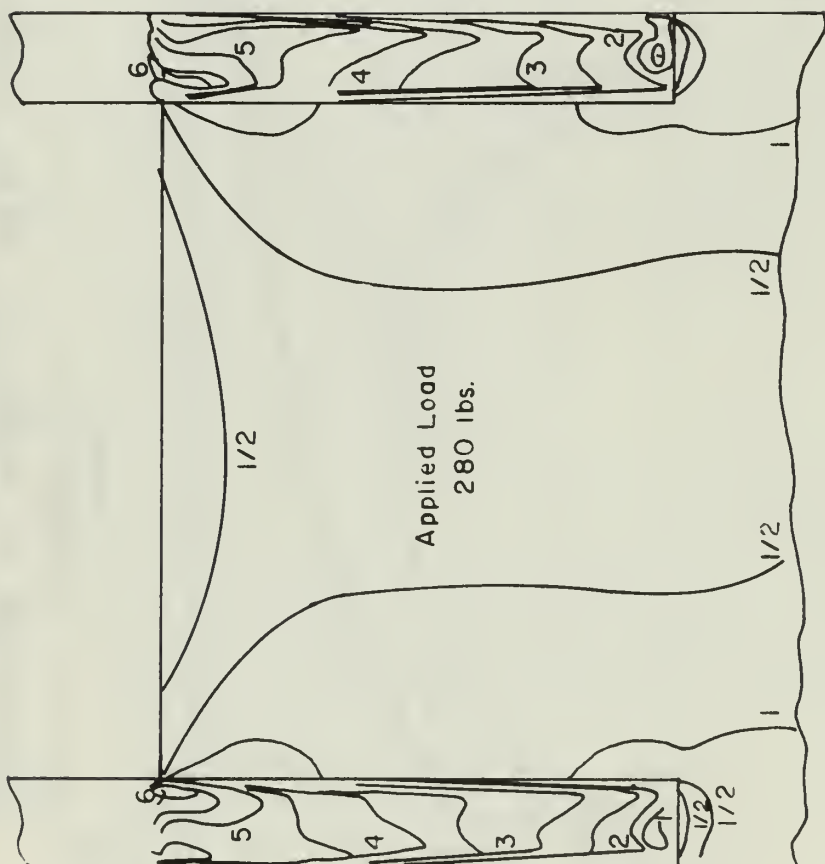


FIGURE 13  
COMPOSITE FRINGE PATTERN  
MODEL TYPE 2

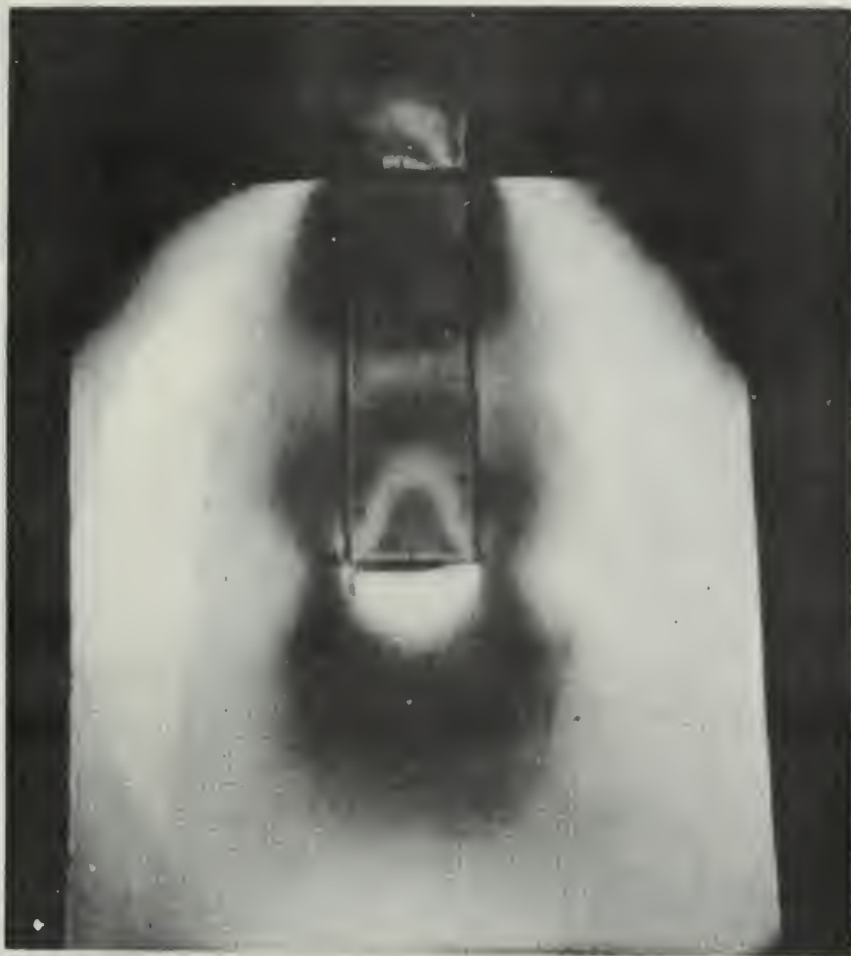


FIGURE 14  
INTEGRAL ORDER FRINGE PATTERN  
MODEL TYPE 1  
250 POUNDS



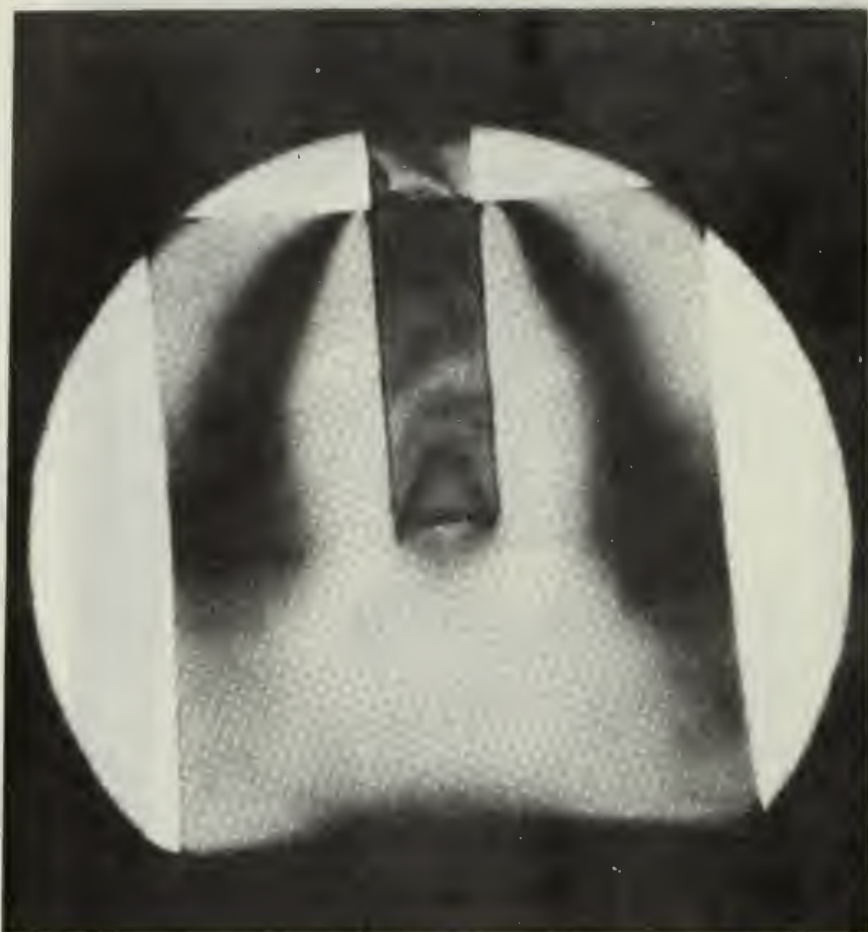


FIGURE 15

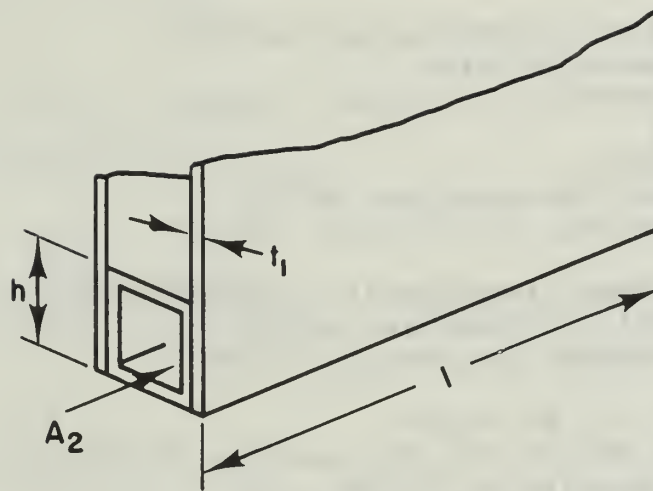
HALF ORDER FRINGE PATTERN  
MODEL TYPE 1  
250 POUNDS



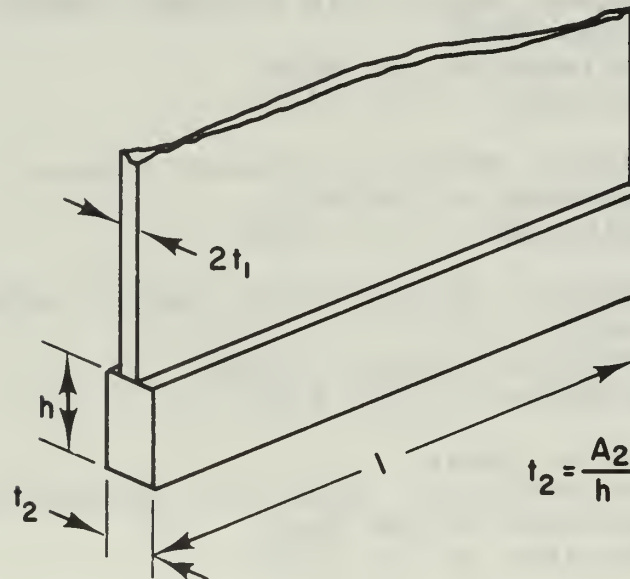
FIGURE 16  
INTEGRAL ORDER FRINGE PATTERN MODEL TYPE 3, 280 POUNDS



FIGURE 17  
HALF ORDER FRINGE PATTERN MODEL TYPE 3, 280 POUNDS



(A) ACTUAL BAR AND SHEET DETAIL



(B) ANALYSIS MODEL

FIGURE 18  
GENERAL DIMENSIONS

# INITIAL DISTRIBUTION LIST

	<u>No. Copies</u>
1. Defense Documentation Center Cameron Station Alexandria, Virginia 22314	20
2. Library Naval Postgraduate School Monterey, California 93940	2
3. Chairman, Department of Aeronautics Naval Postgraduate School Monterey, California 93940	1
4. Prof. C. M. Smith c/o Mechanical Engineering Department University of Toledo Toledo, Ohio 43614	1
5. Captain R. F. Machado 22297 Mission Blvd. Hayward, California 94541	1
6. Commander, Naval Ship Systems Command (Code 0645) Department of the Navy Washington, D. C. 20360	1
7. Commander, Naval Air Systems Command Department of the Navy Washington, D. C. 20360	1
8. Commandant, United States Marine Corps. (A03C) Headquarters Marine Corps Washington, D. C. 20360	1
9. Dr. E. S. Lamar Chief Scientist, Naval Air Systems Command Department of the Navy Washington, D. C. 20360	1
10. Mr. I. Silver Propulsion Administrator, Naval Air Systems Command Department of the Navy Washington, D. C. 20360	1



- |     |                                  |   |
|-----|----------------------------------|---|
| 11. | Mr. G. L. Desmond                | 1 |
|     | Aerodynamics and Structures,     |   |
|     | Naval Air Systems Command        |   |
|     | Department of the Navy           |   |
|     | Washington, D. C. 20360          |   |
| 12. | Prof. A. E. Fuhs                 | 1 |
|     | Department of Aeronautics        |   |
|     | Naval Postgraduate School        |   |
|     | Monterey, California 93940       |   |
| 13. | Prof. H. L. Kohler               | 1 |
|     | Department of Aeronautics        |   |
|     | Naval Postgraduate School        |   |
|     | Monterey, California 93940       |   |
| 14. | Prof. C. H. Kahr                 | 1 |
|     | Department of Aeronautics        |   |
|     | Naval Postgraduate School        |   |
|     | Monterey, California 93940       |   |
| 15. | Mr. J. H. Reinertson (Code 6146) | 1 |
|     | Naval Ship Systems Command       |   |
|     | Washington, D. C. 20360          |   |





## DOCUMENT CONTROL DATA - R&amp;D

(Security classification of title, body of abstract and indexing annotation must be entered when the overall report is classified)

1. ORIGINATING ACTIVITY (Corporate author) Naval Postgraduate School Monterey, California 93940		2a. REPORT SECURITY CLASSIFICATION Unclassified	
		2b. GROUP	
3. REPORT TITLE  Investigation of Shear Lag in Heat Exchanger Module			
4. DESCRIPTIVE NOTES (Type of report and inclusive dates) Master's Thesis			
5. AUTHOR(S) (Last name, first name, initial)  Machado, Robert Francis			
6. REPORT DATE December 1967		7a. TOTAL NO. OF PAGES 63	7b. NO. OF REFS 13
8a. CONTRACT OR GRANT NO.  A. PROJECT NO. N/A  C.  D.		9a. ORIGINATOR'S REPORT NUMBER(S)  N/A  9b. OTHER REPORT NO(S) (Any other numbers that may be assigned this report)	
10. AVAILABILITY/LIMITATION NOTICES <del>Information in this report is classified "Secret" and is to be controlled by the Naval Postgraduate School.</del>			
11. SUPPLEMENTARY NOTES		12. SPONSORING MILITARY ACTIVITY Naval Postgraduate School Monterey, California 93940C.	
13. ABSTRACT  Results of a photoelastic model test which simulates the junction of the closure bar with sheet of a heat exchanger are presented. Values of shear stress 30 per cent above predicted values were found to exist. A linear technique for determination of maximum shearing stress is presented for the purpose of design. Qualitative techniques were employed to compare the results of tests of various photoelastic models.			

UNCLASSIFIED

Security Classification

14

KEY WORDS

LINK A

LINK B

LINK C

ROLE

WT

ROLE

WT

ROLE

WT

SHEAR LAG

HEAT EXCHANGER

BAR SHEET JOINT

PHOTOELASTIC

DD FORM 1473 (BACK)

1 NOV 66

S/N 0101-807-6821

UNCLASSIFIED

Security Classification

A-31409













thesM1892

DUDLEY KNOX LIBRARY



3 2768 00416497 0

DUDLEY KNOX LIBRARY